Dynamic Characterization of Hydroelectric Turbine with Transient Data Records Using OBMA and Phase-Shift Analysis

Quentin DOLLON[1], Antoine TAHAN[2], Jérôme ANTONI[3], Martin GAGNON[4], Christine MONETTE [5]

[1]ÉTS, Montréal, INSA Lyon
quentin.dollon.1@ens.etsmtl.ca
[2] ÉTS, Montréal, Dpt. Mécanique, H3C 1K3, Montreal, Qc., Canada
antoine.tahan@etsmtl.ca
[3]Univ Lyon, INSA-Lyon, Lab. Vibrations Acoustique, F69621 Villeurbanne, France
jerome.antoni@insa-lyon.fr
[4]Institut de Recherche de HydroQuébec (IREQ), J3X 1S1, Varennes, Qc., Canada
gagnon.martin11@ireq.ca
[5]Andritz Hydro Ltd., H9R 1B9, Pointe-Claire, Qc., Canada
christine.monette@andritz.com

Abstract

The purpose of this paper is to investigate the possibility of estimating Francis hydroelectric turbine modal parameters in transient conditions by focusing on resonance regions generated by the interaction of a structural mode with a frequency-variant harmonic pressure pulsation. Especially when numerous modes are in the same bandwidth, this method separates them by exciting only matching mode shapes. To extract a specified harmonic from the signal, the resonance retrieval is done using Order Tracking method. A classical ambient modal identification algorithm is then used to feature the isolated mode. Furthermore, using the phase-shift between measured locations, modes can be localized and shape determined.

List of Symbols

i	Complex unit	ω_k	Discrete pulsation $k \in [\![1, N_f]\!]$
$diag[\boldsymbol{A}]$	Diagonal matrix of vector $\boldsymbol{A}$	$\widehat{\boldsymbol{X}}_k$	$(N_S \times 1)$ Estimated frequency response in ω_k ($\mathbb{C}$)
$<\boldsymbol{A}\|\boldsymbol{B}>$	Complex inner product of $\boldsymbol{A}, \boldsymbol{B}$	$\boldsymbol{X}_k$	$(N_S \times 1)$ Theoretical frequency response in ω_k ($\mathbb{C}$)
$\boldsymbol{A}^T$	Transpose of $\boldsymbol{A}$	$h_{r,k}$	Modal transfer function of mode r in ω_k ($\mathbb{C}$)
$\boldsymbol{A}^*$	Conjugate of $\boldsymbol{A}$	p_k	Scaled FFT of modal Excitation in ω_k ($\mathbb{C}$)
$\|\boldsymbol{A}\|$	Determinant of $\boldsymbol{A}$	$\boldsymbol{\varepsilon}_k$	$(N_S \times 1)$ Scaled FFT of channel noise in ω_k ($\mathbb{C}$)
δ_r	Kronecker Symbol	$\boldsymbol{E}_k$	$(N_S \times N_S)$ Theoretical density matrix in ω_k ($\mathbb{C}$)
N_S	Number of sensors	$s_{1,k}$	First singular value of E_k
N_f	Number of frequency samples		
		$\boldsymbol{\varphi}_r$	$(N_S \times 1)$ Theoretical mode shape of mode r ($\mathbb{C}$ in FDD)
$\boldsymbol{\Phi}$	$(N_S \times n)$ Global modal matrix for a system of n modes	$\widehat{\boldsymbol{\varphi}_r}$	$(N_S \times 1)$ Estimated mode shape of mode r
MAC	Modal Assurance Criterion	β_r	Characteristic real scalar value of mode r
MAC_{thr}	Threshold MAC in E-FDD	ω_r	Natural pulsation of mode r
$\boldsymbol{\theta}_r$	$(4+N_S \times 1)$ Parameter vector of mode r	ξ_r	Damping Ratio of mode r
$\boldsymbol{\theta}$	$(4+N_S \times 1)$ Modal parameter vector as a variable	S_r	Modal force of mode r
$\mathscr{L}(\boldsymbol{\theta})$	Negative Log-Likelyhood Function	S_{er}	PSD Error for mode r

1 Introduction

Design and exploitation of hydroelectric turbines relies on the knowledge of their dynamic behavior. This enables one to generate and validate models to either get a good assessment of life duration or plan predictive-based maintenance. Two sources of information are useful to properly characterize the mechanical behavior of a structure: numerical simulations and experimental data processing. Giving high computing power, the first

source could give a whole and detailed analysis of the behavior in any expected regime through Computational Fluid Dynamics (CFD) and Finite Element Analysis (FEA) but needs to be validated by the second to be reliable. It is a straightforward consequence of the strong assumptions made to reduce computational burden and model the highly turbulent characteristics of the flow. The second approach relies on in-situ measurements to extract dynamic features [1].

The increase of computational power over years allows getting more accurate simulations for startup regimes [2, 3], no-load or part-load configurations [4, 5, 6] and even hydrodynamic damping estimations [7]. However, the results still show discrepancies in structural parameters due to deviations from real operating conditions: rotating machinery [8], fluid-structure interaction added mass, damping and stiffness [9, 10], cavitation influence [11, 12, 13] or boundary condition sensitivity [14]. On the other hand, experimental characterization is highly fragmented, but in general closer to reality for a given measured operating condition. The features obtained from experimental data relie on statistical models [15, 16], indirect measurements [17], time-frequency analysis [18], but can also be obtained by modal parameter identification using Operational Modal Analysis (OMA) [19] or Experimental Modal Analysis (EMA) [20]. In addition, the experimental hydraulic instability study can be used to compare different computational turbulence models [21, 22, 23]. Typically, the two sources of information (simulations and experiments) are crossed to obtain a hybrid representation of the dynamic behavior, which is used to obtain accurate load levels and allow a better prediction of fatigue [24]. Those predictions are used to assess the runner life duration and reliability of the capacity [25, 26, 27].

One of the problems with experimental analysis is the cost of data acquisition. To reduce financial burden of measurements, the idea is to extract a maximum of information from transient records instead of several stationary records, which would make the measurement less time-consuming. Furthermore, the processing of transient records allows obtaining real structural parameters of highly damaging regimes [23, 28] (what numerical analysis still struggles to perform, as aforementioned). Our goal is to determine whether a signal processing methodology is able to extract precise and suitable features from these transient measurements. For this, a combined methodology using Order Tracking, OMA and Phase-Shift Analysis is implemented and performed on a case study. The case study data come from a medium-head Francis Turbine in Quebec (Canada). The paper first presents the theoretical background, including literature and the different OMA tools to be used. Afterwards, the model is tested on the case study of an operational runner prototype.

2 Resonance Detection Using Phase-Shift Diagrams

Resonances are usually found with the study of experimental correlograms where the amplified regions are treated as Operating Deflecting Shape (ODS). But there is another alternative to detect resonances with more confidence: Phase-Shift Analysis (PSA) [29, 30]. Resonance amplitudes are time-dependent and phases are relative to a reference in experimental data, but the modal phase-shift from one sensor to another is a theoretical time invariant absolute quantity that is specific to each mode. Especially, when a harmonic (time-variant pulsation) and a mode (almost constant pulsation) intersect with the same phase-shift, the observed ODS is very likely the resonance of the only excited mode. This resonance can be extracted and processed with OBMA through a Single Degree of Freedom (SDoF) formulation (Section 3 & 4). Once the mode has been detected, it is possible to feature its shape: the mode shape is assumed to be the nodal diameter that fits the best the modal phase-shift (e.g. [18] in which a self-excited vibration of a hydroelectric runner is studied during load rejection). It is also possible to determine the shape by identifying the pattern of the exciting harmonic, particularly if this last comes from a well-known phenomenon (vortex rope [27, 31, 32, 33, 34], Rotor-Stator Interactions (RSI) [26, 27, 31, 35, 36]).

3 Order Tracking Procedure

Once PSA and resonance mapping is achieved, it is still required to extract accurate damping ratios and frequencies, and eventually other modal properties (modal force *etc.*). In order to do this, identification algorithms are implemented to process multi-channel resonance signals. The first pre-processing step is to extract the resonance component and isolate it from the rest of the signal. This is the purpose of Order Tracking. This class of method gathers all the tools able to extract one harmonic from the signal by shifting the time

domain to a harmonic one, called order domain. Orders, measured in times per revolution, are analog to frequencies. Order Tracking is a classical and very used diagnosis tool for rotating machineries. There are four main techniques that are commonly used: direct method using Fourier Transform of a time series (FS), Angular Resampled-based Order Tracking (AD), Time-Variant Discrete Fourier Transforms (TVDFT) and Vold-Kalman filters (VK).

FS extracts the $n-th$ harmonic from a signal by tracking the $\widehat{\boldsymbol{X}}[n\omega_{0,k}]$ response with a short-time Fourier transform at each time step, where $\omega_{0,k}$ is the runner angular velocity at time step k. This procedure is highly biased due to tapering, leakage effects and bandwidth control. In the classical approach with constant time intervals, low rotating frequencies are less accurate than higher ones. If time intervals are non-constant, some power spectral density rescaling issues rise and must be taken into account.

Another technique relies on an adaptative Fourier transform with settable kernel [37]: the kernel of the analytic exponential function tracks the frequency of interest. Consequently, a precise targeted order is extracted. In early works, the kernel orthogonality was lost and a compensation matrix had to be introduced to partly fix the problem. This issue is now easily fixed by introducing a change of variable in the integration domain, and gives a Velocity Synchronous Fourier Transform [38]. Vold-Kalman (VK) Bank Filters can extract orders from a signal with an instantaneous analysis instead of an averaging procedure [39]. Consequently, VK filtering is the most accurate technique in terms of resolution but entails a heavy computational burden, that is irreconcilable with industrial applications.

AD is a resampled-based method that avoids any leakage effect and phase issues [40]. The asynchronous time series are turned into synchronous time series (constant $\Delta\alpha$ instead of Δt) by the means of interpolation and tachometer record (Computed Order Tracking [41]). Then, a short-time Fourier transform is performed on the resampled signal, with intervals corresponding to one runner revolution (so that the spectrum resolution coincides with orders). Intervals are neither overlapped nor windowed. An order spectrum is obtained for each studied revolution. Each of those revolutions is converted into frequency by averaging the rotational speed over the lap. It can be noticed that the lower the studied dynamic, the weaker the quasi-static assumption over a revolution, the higher the response estimation quality. The bias of AD comes from both interpolation and synchronous interval split. Interpolation bias is due to interpolating method (*e.g.* linear, quadratic, splines) and shaft torsion that induces tachometer signal fluctuations. The issue with synchronous interval split is that each interval must represent exactly one revolution, that is not necessarily the case. Most of those biases can be reduced if data are recorded with a extensively high sampling frequency compared to the structure natural frequencies. For the purpose of this paper, the classical COT-based AD will be used, because the data sampling frequency is far higher than the natural frequencies of studied modes.

4 Operational Modal Analysis

Few has been done in the field of OMA for hydroelectric runner dynamic featuring. Gagnon et *al.* used this technique to characterize guide-vane behavior for different operating conditions [19]. The same point is made for EMA for which the study achieved on a runner obtained results that were in well agreement with simulations, but for experimental setting not representative of actual operating conditions [20]. Moreover, in many cases EMA cannot be implemented and when it is possible, suffers from major drawbacks like experimental set-up cost or structural size and complexity. The point of OMA is to extract modal parameters from output-only measurements containing both unknown excitation and response of the system. When those signals are extracted with Order Tracking, the procedure is called OBMA (Order Based Modal Analysis) [40, 42, 43, 44]. OMA is of interest for several reasons: it is fast in terms of computing effort and measurement (mere sensors replace excitation set-up), ambient excitation is appropriate to linearize the dynamic behavior and so on.

OMA techniques are divided into different classes: they can process in the time domain (TD) or frequency domain (FD), and can be parametric or non-parametric [45]. TD approaches are straightforward, and are generally parametric. They mainly study the auto-regression degree with (AR)MA-(X) models [46] and Subspace Identification technics [47] or the output correlations between channels (Polyreference, LSCE, Subspace Identification, ERA) [48]. Frequency approaches can be parametric (Polymax or Polyreference) [49] or non-parametric (Pick- Peaking, (E)-FDD) [50, 51]. Non-parametric methods often rely on Single Degree of Freedom (SDoF) theory, so that a pre-processing step is mandatory to separate modal contributions.

In OBMA, Polymax model has typically been implemented as identification support [40, 42]. However,

Polymax does not seem to be the best candidate for such an identification, because parametric models always generate spurious modes (due to noise and numerical bias). Furthermore, the model order is always difficult to define (methods are based on stabilization diagrams or parsimony principle through the minimization of criteria, *e.g.* Akaike and Bayesian Information Criterion, AIC or BIC). In order-tracked signals, it is easy to know in advance the number of excited modes, which allows using non-parametric methods. Thus, the authors propose to perform the following procedure: different modes are decomposed into SDoF responses and bandlimited using a partial E-FDD procedure. Then, each mode is identified using a classical ambient SDoF transfer function with a maximum likelihood estimator.

4.1 SDoF Separation

SDoF separation is performed using a modal coherent criterion applied on the singular vectors of the discrete spectral density matrix. The classical input-output relation of density matrices under the condition of white-noise input, low damping and uncoupled modes, can be developed according to the Heaviside partial-fraction expansion theorem in the vicinity of its modal pulsations [52, 53].

$$\boldsymbol{E}_k|_{\omega_k \approx \omega_r} \approx \boldsymbol{\Phi}^* diag\left[\frac{\beta_r}{(\xi_r \omega_r)^2}\delta_r\right]\boldsymbol{\Phi}^T \tag{1}$$

Eq. 1 shows that the excitation density matrix is diagonal, and thus the output density matrix E is equivalent to a diagonal one. The change of basis is done with the modal matrix $\boldsymbol{\Phi} = (\boldsymbol{\varphi}_1, ...\boldsymbol{\varphi}_n)$. The diagonal matrix contains only one non-zero term expressed as the contribution of the investigated mode through $(\beta_r, \xi_r, \omega_r)$, respectively a characteristic scalar value, the damping ratio and the natural pulsation of mode r. The Kronecker symbol δ_r is 1 for the $r-th$ position of the diagonal matrix, else 0. In the vicinity of a natural pulsation, the associated mode is the only contributor to the global dynamic of the system. The associated mode shape is $\boldsymbol{\varphi}_r$, $r-th$ column of $\boldsymbol{\Phi}$. In other terms, it is shown that the Singular Value Decomposition of the experimental density matrix in the vicinity of a mode returns only one dominant singular value. The associated singular vector in $\omega_k = \omega_r$ (within the limit of frequency resolution) is the mode shape estimator. The set of the first singular values $\{s_{1,k}\}$ is called Complex Modal Identification Function (CMIF) and is a unilateral representation of the previous spectral density functions. The resonance function of each SDoF is identified from the CMIF thanks to a discriminating criterion, the Modal Assurance Criterion (MAC) [54]. MAC varies from 0 to 1 as the modal coherence increases. It compares the degree of agreement of two vectors:

$$MAC(\boldsymbol{\varphi}_i, \boldsymbol{\varphi}_j) = \frac{<\boldsymbol{\varphi}_i|\boldsymbol{\varphi}_j>^2}{<\boldsymbol{\varphi}_i|\boldsymbol{\varphi}_i><\boldsymbol{\varphi}_j|\boldsymbol{\varphi}_j>} \tag{2}$$

This criterion is able to separate two uncoupled close modes and discriminate spike noises. Brinker et *al.* set the threshold to $MAC_{thr} = n/\sqrt{N_S}$, where n is an integer so that MAC_{thr} is close but lower than 1, and N_S the number of studied sensors [55]. If $MAC(\widehat{\boldsymbol{\varphi}_r}, \boldsymbol{\varphi}_j) > MAC_{thr}$, where $\widehat{\boldsymbol{\varphi}_r}$ is the shape estimator and $\boldsymbol{\varphi}_j$ a singular vector of the CMIF, then $s_1[\omega_j]$ belongs to the resonance function of the SDoF. This ensures to select a bandwidth with high modal coherence. Figure 1 shows an example of the use of MAC. The E-FDD theory shifts back in time domain to make the identification. But this procedure is a bad damping estimator, especially in the case of short signals [56]. For this reason, the identification support is different and presented in the next subsection.

A last point can be raised about the E-FDD limits: this procedure is only proper to separate uncoupled signals. In the case of coupled modes, it is unable to differentiate modal contributions. In future works, a Frequency-Domain Blind Source Separation developed by Castiglione et *al.* should be used instead [57]. FD-BSS is able to separate coupled modes with an impressive accuracy, and relies on a more rigorous mathematical approach.

4.2 Identification Using Maximum Likelyhood

After being extracted using AD method and bandlimited with MAC, the N_S experimental frequency responses are concatenated into a vector $\widehat{\boldsymbol{X}}_k$ and are modelled with the classical SDoF response described in eq. (3, 4), where $\boldsymbol{X}_k$ is the theoretical response vector, $h_{r,k}$ is the modal transfer function depending on modal parameters (ω_r, ξ_r) and $p_k, \boldsymbol{\varepsilon}_k$ are the normalized Fourier transforms of excitation and noise respectively.

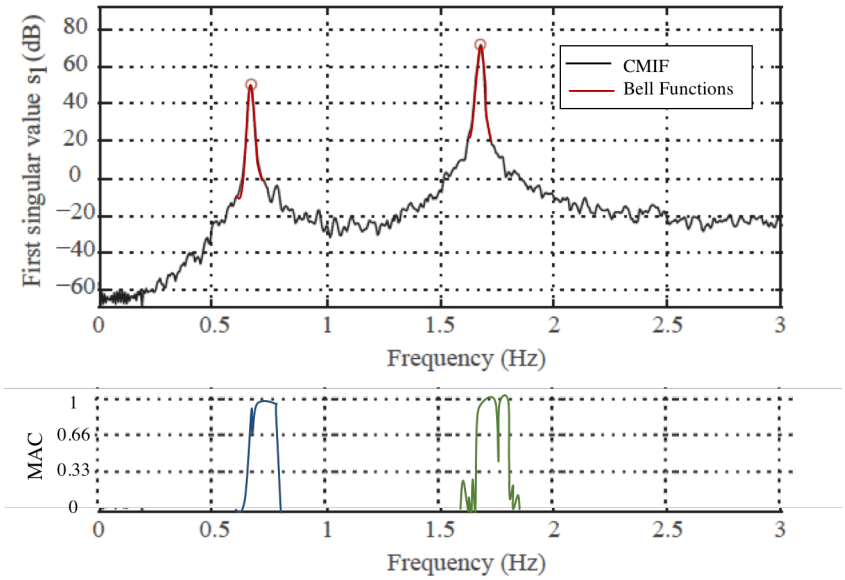

Figure 1: Modal contributions are framed using MAC, which compares the agreement level between two mode shapes.

$$\boldsymbol{X}_k = \boldsymbol{\varphi}_r h_{r,k} p_k + \boldsymbol{\varepsilon}_k \tag{3}$$

$$h_{r,k} = -\frac{1}{\omega_k^2 - \omega_r^2 - 2i\xi_r \omega_r \omega_k} \tag{4}$$

The associated Negative Log-Likelihood Function (NLLF) is given in eq. (5), where N_f is the number of point per channel, $\boldsymbol{E}_k[\boldsymbol{\theta}]$ the theoretical SDoF density matrix arising from eq. (3) and $|\boldsymbol{E}_k[\boldsymbol{\theta}]|$ the determinant of the density matrix ; the analytical determination of both determinant and inverse matrix of $\boldsymbol{E}_k[\boldsymbol{\theta}]$ is far from being trivial, and described in [58]. $\boldsymbol{\theta}_r = (\omega_r, \xi_r, S_r, S_{er}, \boldsymbol{\varphi}_r)$ is the parameter vector, including natural pulsation, damping ratio, modal force, PSD error and mode shape. $\boldsymbol{\theta}$ is the parameter variable, used to estimate $\boldsymbol{\theta}_r$. The NLLF is minimised using a Nelder-Mead algorithm [59]. A such identification method was chosen because it shows the best asymptotic properties.

$$\mathscr{L}(\boldsymbol{\theta}) = N_S N_f ln(\pi) + \sum_{k=1}^{Nf} ln(|\boldsymbol{E}_k[\boldsymbol{\theta}]|) + \sum_{k=1}^{N_f} \widehat{\boldsymbol{X}}_k^* \boldsymbol{E}_k^{-1}[\boldsymbol{\theta}] \widehat{\boldsymbol{X}}_k \tag{5}$$

5 Case Study

The studied measurements come from a vertical medium head Francis hydroelectric runner exploited in Quebec, Canada. This facility was chosen because the turbine was designed and is operated by two partners of the current project. The measurement data were recorded during a slow transient from no-load overspeed to stop. Two blades separated with an angle of 111° were instrumented with strain gauges. Intrados were instrumented with three strain gauge rosettes, located in the band junction to blade leading edge and trailing edge, and in the middle crown-blade weld, as shown in Figure 2. Extrados were instrumented with two uniaxial gauges, one close to the crown, the other close to the band. The locations are the same from one blade to another to ensure a redundant signal. Accelerometers and pressure sensors are located in different points (blade, structure and penstock) and sensors are also installed on the shaft to record torque, flexion and thrust. The rosette and uniaxial gauges are oriented in agreement with the expected strain flow direction, *.e.* in the direction of the principal stresses.

An analysis of experimental correlograms (amplitude of short-time Fourier transforms) and absolute phase-shift spectra between redundant sensors was made first. Some examples are shown in Figures 3 and 4, related to

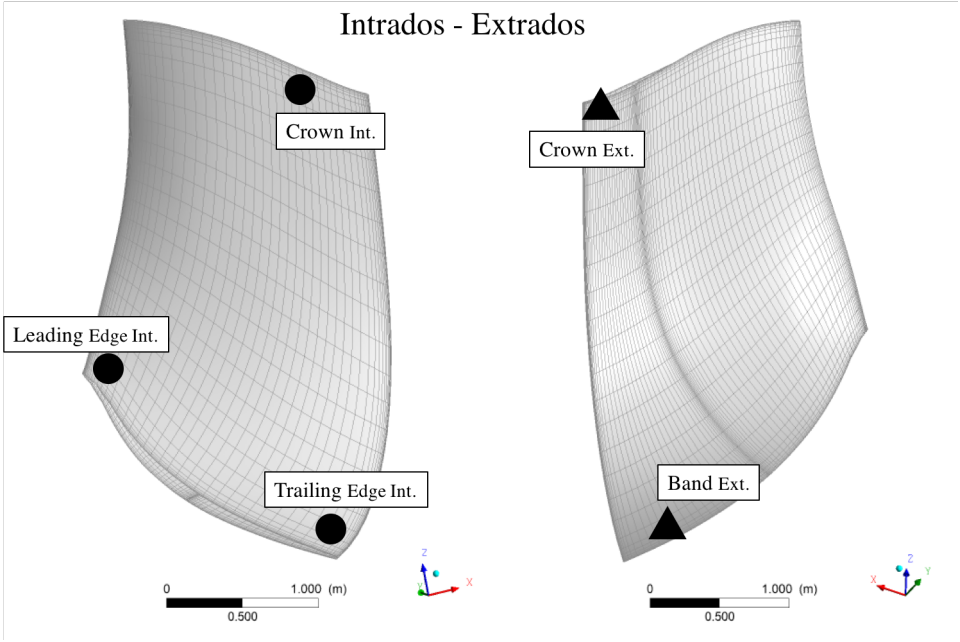

Figure 2: Strain gauge location on the instrumented blades. Circles represent rosette gauges, triangles represent uni-axial gauges.

both sides of the crown (time and frequency axes are empty for the purpose of clarity). When the windowing is long enough, correlograms show five ODS. Several modes can be contained inside. A clear resonance of mode 1 is detected on the intrados in the lower part of the diagram (below blade passing frequency signature, abusively denoted "RSI") ; the other resonances are in the upper part. Phase-Shift spectra are amplitude-filtered, and show only phases associated with a high enough correlogram. They show four single-mode bands and a multi-mode band, due to multiple phase-shift detection. Resonance of mode 2 is detected on both sides, and mode 3 is vaguely detected on the extrados. Only one mode of the multi-shifted band is excited by a harmonic, thus leading to a SDoF resonance. Table 1 summarizes all the detected modes in the range $[0, 100]Hz$, and reports the related resonant harmonic index. Phase-shifts are averaged over the region where the mode is found.

In the studied data, all the time series are recorded with an extensively large sampling frequency, and the use of AD technique to extract harmonics should be straightforward. The next subsections present typical case studies based on previous identified modes.

Mode Reference	Frequency [Hz]	Phase-Shift $\times\pi$[rad]	Harm. Order
1	18.0	0	13
2	28.0	$\pm$3/4	42
3	50.0	$\pm$1/7	63
4	91.0	$\pm$1/9	$\emptyset$
5	58.0	$\pm$6/7	61

Table 1: Experimentally Detected Modes

5.1 Identification Example: Shaft Torsion Mode with $f_0 = 18Hz$

The first mode to be studied, mode 1, is excited by the $13-th$ harmonic of the rotating speed. This corresponds to the blade passing frequency. Such an excitation can come for instance from the spiral case intake or the drat tube elbow that can create a stationary disturbance that is seen by the rotating runner each time a blade passes in front of the intake or the draft tube direction. The investigation of torsion measurements shows that the studied mode is a natural torsion mode of the shaft line. What is observed on blades is only the propagation of shaft natural vibrations. Thus, all the runner is excited with the same phase, and the nodal diameter is 0, that

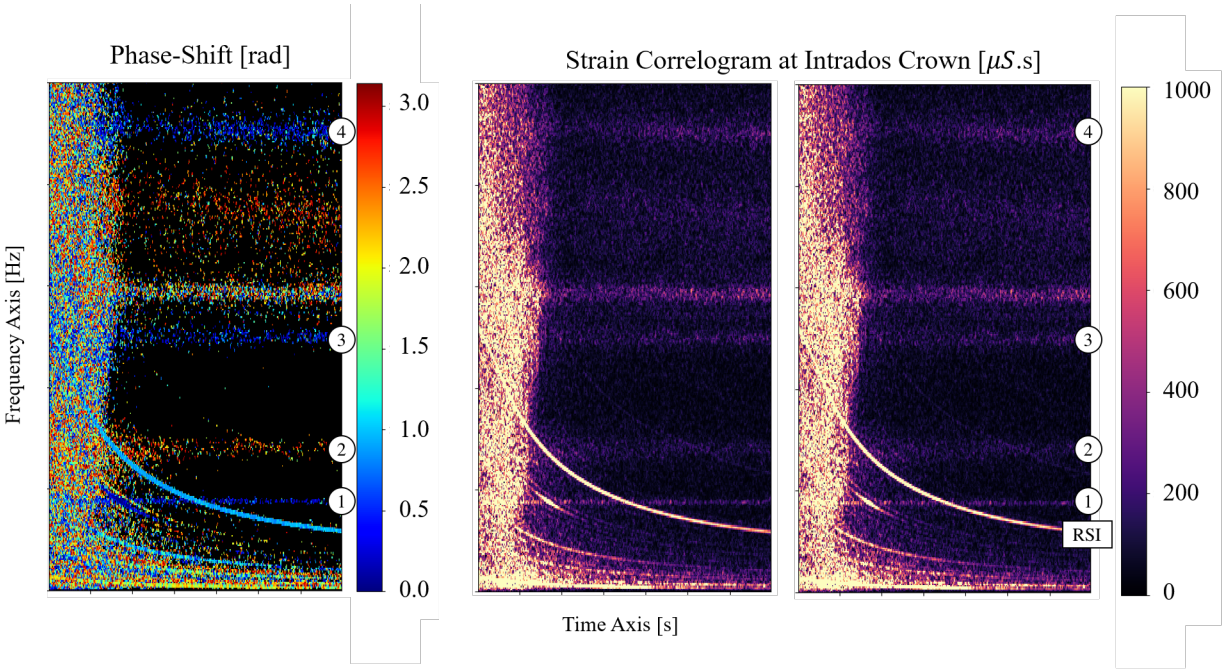

Figure 3: ODS Analysis of principal direction of intrados crown Rosette gauge. On the left, phase-shift spectrum of the redundant gauges. On the right, redundant amplitude spectra.

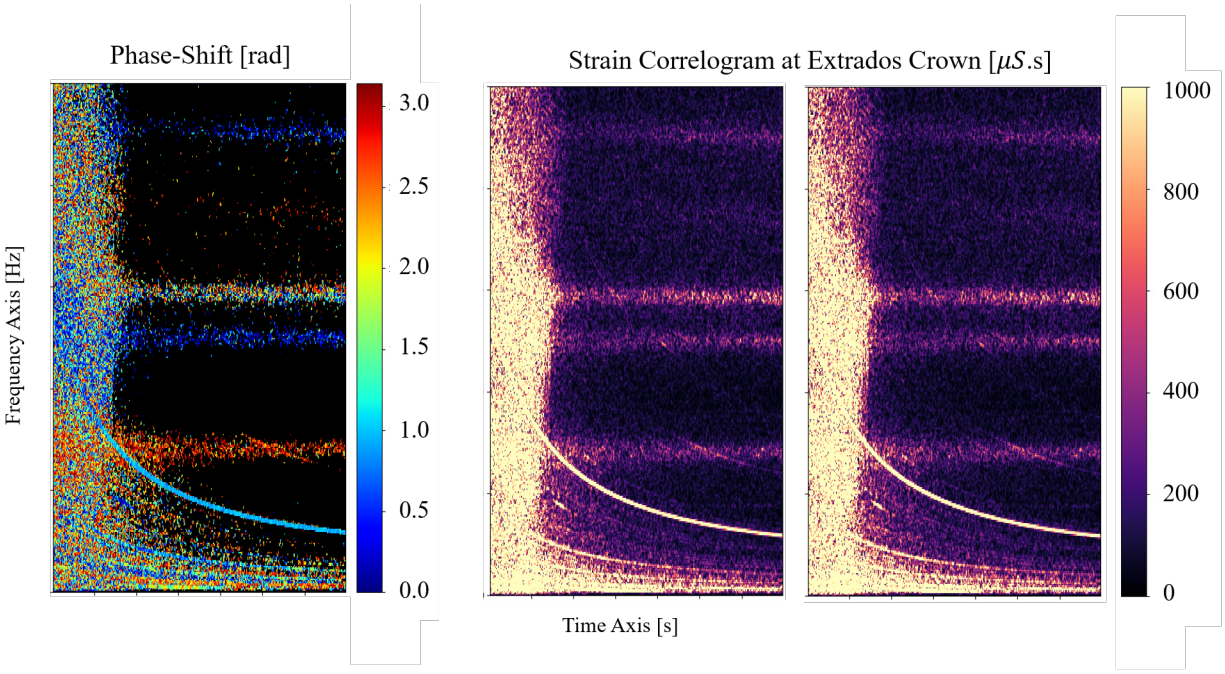

Figure 4: ODS Analysis of extrados crown Rosette gauge.

is confirmed by the absence of phase-shift between blades. An axial thrust pulsation is measured on the shaft, and indicates that the inflow to the runner is not symmetric to the guide vane orientation [31]. Examples of extracted resonances are shown in Figure 5. The *MAC* narrows the bandwidth with a threshold $MAC_{thr} = 0.875$, as depicted in Figure 6. The maximum likelihood estimator raises optimal parameters, shown in Table 2 and Figure 7.a.

Natural Frequency	Damping Ratio	Modal Force	PSD Error
f_0 [Hz]	ξ [%]	S [ms^2/Hz]	S_e [μ S/Hz]
17.43	1.26	2.22E6	1.73E-2

Table 2: Torque Mode Featuring

The shape relative amplitudes are the same on the two blades, as testifies Figure 7.a.. The mode shape is in phase opposition from leading edge to crown, and is not spotted neither on trailing edge intrados or on band extrados signals. That attests a $ND-0$ "in umbrella", as depicted in Figure 7.b. The modal force is very difficult to extract and is likely very biased. The bias on damping ratio mainly depends on experimental data. The leakage and tapering bias due to the windowing is avoided thanks to COT-based AD. However, the global uncertainty level remains likely high because of the unknown excitation.

5.2 Results

Table 3 shows the result of the identification process performed on all detected resonance harmonics. The information presented is: the exciting harmonic (indexed on the rotating frequency), the most likely nodal diameter, the Signal-to-Noise Ratio (SNR), the bandwidth and the associated method (*MAC* or SENS for sensitivity analysis) and the modal parameters. Except for the torsion mode, resonance signals have a low SNR that renders impossible the use of *MAC*, because the singular value spectrum is still buried in noise. Instead, a sensitivity analysis was made on modal parameters as a function of the bandwidth. The selected band corresponds to the parameter convergence. This method gives wider bands (around ten times the width of a *MAC* selected bandwidth), where noise has a significant influence. Rather, *MAC* criterion selects a narrower frequency band with very few noise. The two methods return quite equivalent results. The experimental data reveals five isolated modes numbered from 1 to 4 in Figure 4, and a multi-mode band. Amongst the 4 well-separated modes, only the first 3 are excited by a harmonic and then identifiable. Into the multi-mode band, one mode is excited by a harmonic. It is thus possible to feature it, but the SNR is particularly low. Notice that the first mode of table 3 is the torsion mode featured in table 2.

6 Conclusion

This paper shows that Francis runner structural modes can be identified from ambient vibration data during transient conditions. These modes have been successfully extracted and identified through an enhanced OBMA technique (E-OBMA). E- OBMA combines three existing techniques and takes benefit from the best of each: Order Tracking separation quality, MAC bandlimiting rigor and maximum likelihood accuracy. This work shows that experimental transient data contains accurate frequency information that can be used to assess numerical model validity. The presented results are the first effort in creating OMA strategy tailored for Francis runners. The E-OBMA still has to be validated on an analytical case, which is now being developed. The Order Tracking quality should be evaluated in conjunction with EMA sine-sweep excitation theory. Also, further improvements will make possible the uncertainty quantification which is a major stake in signal processing.

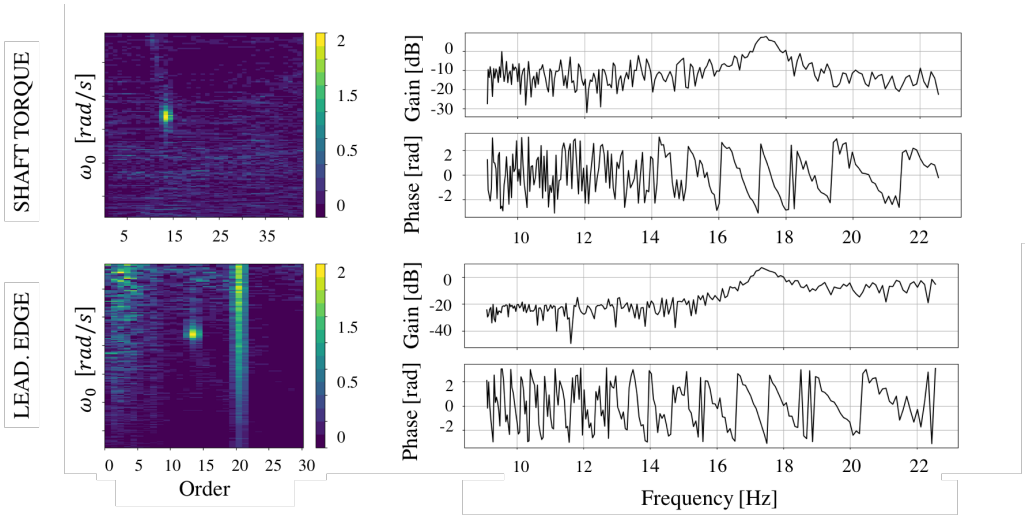

Figure 5: On the left, Order Spectra. All the harmonic contents are on the same line. On the right, the related Bode Diagrams of the harmonic 13.

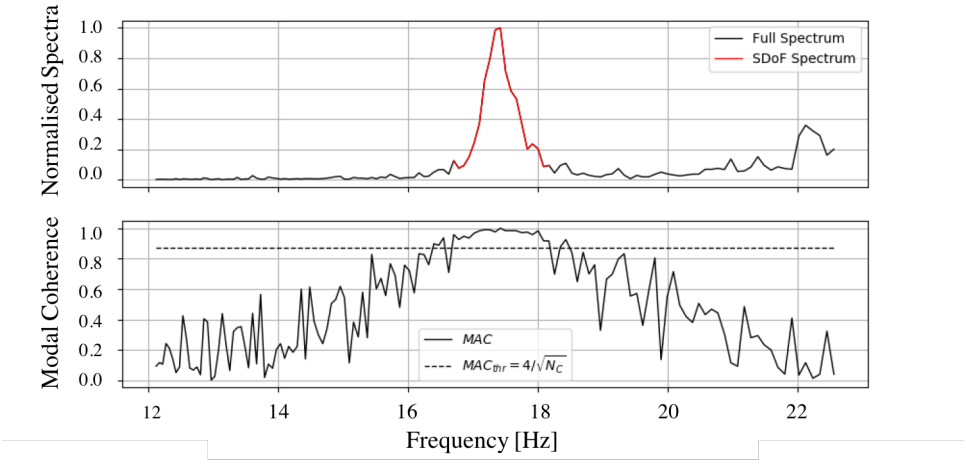

Figure 6: Resonance function extraction from the first singular values spectra (CMIF).

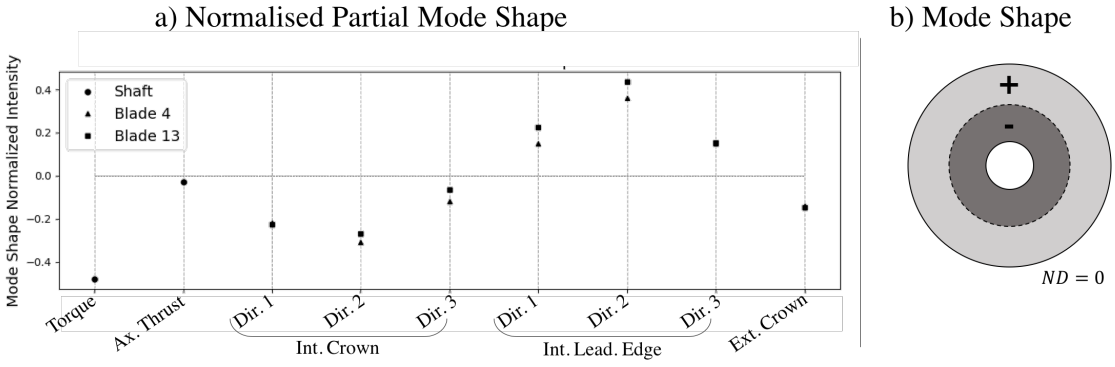

Figure 7: a) Partial mode shape extracted with maximum likelihood. b) Schematics of the observed mode shape.

		Identification BandWidth	Modal Parameters	
Mode	Nodal Diameters	Bandwidth (Hz)	Frequency (Hz)	Modal Force (ms^2/Hz)
Harm. Index	SNR (dB)	Method	Damping ratio (%)	PSD Error (μ s/Hz)
1	0	1.5	17.43	2.22E6
13	7.4	MAC	1.26	1.73E-2
2	1	8	28.71	3.31E5
42	1.8	SENS	3.26	1.18E-3
3	3/5	9	49.84	1.40E6
63	1.9	SENS	1.67	8.00E-4
Multi.	6	12	59.35	4.31E6
61	0.96	SENS	2.30	2.00E-3

Table 3: OBMA Identification Results

References

[1] A. Presas, Y. Luo, Z. Wang, and B. Guo. Fatigue life estimation of francis turbines based on experimental strain measurements: Review of the actual data and future trends. *Renewable and Sustainable Energy Reviews vol. 102*, page 96 to 110, March 2019.

[2] J. Nicolle, J.F. Morissette, and A.M. Giroux. Transient cfd simulation of a francis turbine startup. *IOP Conf. Ser.: Earth Environ. Sci. vol. 15 062014*, October 2012.

[3] J. Nicolle, A.M. Giroux, and J.F. Morissette. Cfd configurations for hydraulic turbine startup. *IOP Conf. Ser.: Earth Environ. Sci. vol. 22 032021*, September 2014.

[4] T. Krappel, A. Ruprecht, S. Riedelbauch, R. Jester-Zuerker, and A. Jung. Investigation of francis turbine part load instabilities using flow simulations with a hybrid rans-les turbulence model. *IOP Conf. Ser.: Earth Environ. Sci. vol. 22 032001*, March 2014.

[5] B. Nennemann, J.F. Morissette, J. Chamberland-Lauzon, and C. Monette. Challenges in dynamic pressure and stress predictions at no-load operation in hydraulic turbines. *IOP Conf. Ser.: Earth Environ. Sci. vol. 22 032055*, 2014.

[6] J.F. Morissette, J. Chamberland-Lauzon, B. Nennemann, C. Monette, A.M. Giroux, A. Coutu, and J. Nicolle. Stress predictions in a francis turbine at no-load operating regime. *IOP Conf. Ser.: Earth Environ. Sci. vol. 49 072016*, July 2016.

[7] B. Nennemann, C. Monette, and J. Chamberland-lauzon. Hydrodynamic damping and stiffness prediction in francis turbine runners using cfd. *IOP Conf. Ser.: Earth Environ. Sci. vol. 49 072006*, page 854 to 865, July 2017.

[8] A. Presas, D. Valentin, E. Egusquiza, C. Valero, and U. Seidel. Influence of the rotation on the natural frequencies of a submerged-confined disk in water. *Journal of Sounds and Vibrations vol. 337*, page 161 to 180, February 2015.

[9] C. Trivedi and M.J. Cervantes. Fluid-structure interactions in francis turbines: A perspective review. *Renewable and Sustainable Energy Reviews vol. 68*, page 87 to 101, February 2017.

[10] A. Presas, D. Valentin, E. Egusquiza, C. Valero, M. Egusquiza, and M. Bossio. Accurate determination of the frequency response function of submerged and confined structures by using pzt-patches. *Sensors*, March 2017.

[11] A. Ducoin, J. Andre-Astolfi, and J.-F. Sigrist. An experimental analysis of fluid structure interaction on a flexible hydrofoil in various flow regimes including cavitating flow. *European Journal of Mechanics - B/Fluids vol. 36*, page 63 to 74, December 2012.

[12] A. Lelong, P. Guiffant, and J.A. Astolfi. An experimental analysis of the structural response of flexible lightweight hydrofoils in cavitating flow. *Journal of Fluids Engineering vol. 140*, November 2017.

[13] X. Liu, Y. Luo, A. Presas, Z. Wang, and L. Zhou. Cavitation effects on the structural resonance of hydraulic turbines: failure analysis in a real francis turbine runner. *Energies vol. 11*, September 2018.

[14] D. Valentin, D. Ramos, M. Bossio, A. Presas, E. Egusquiza, and C Valero. Influence of the boundary conditions on the natural frequencies of a francis turbine. *IOP Conf. Ser.: Earth Environ. Sci. vol. 49 072004.*, November 2016.

[15] M. Gagnon, A. Tahan, P. Bocher, and D. Thibault. On the stochastic simulation of hydroelectric turbine blades transient response. *Mechanical Systems and Signal Processing vol. 32*, page 178 to 187, October 2012.

[16] M. Poirier, M. Gagnon, A. Tahan, A. Coutu, and J. Chamberland-Lauzon. Extrapolation of dynamic load behaviour on hydroelectric turbine blades with cyclostationary modelling. *Mechanical Systems and Signal Processing vol. 82*, page 193 to 205, January 2017.

[17] I. Diagne, M. Gagnon, and A. Tahan. Modeling the dynamic behavior of turbine runner blades during transients using indirect measurements. *IOP Conf. Ser.: Earth Environ. Sci. vol. 49 072014*, July 2016.

[18] E. Moisan, D.-B. Giacobbi, M. Gagnon, and F. Leonard. Self-excitation in francis runner during load rejection. *IOP Conf. Ser.: Earth Environ. Sci. vol. 22 032025*, September 2014.

[19] M. Gagnon, A. Tahan, A. Coutu, and M. Thomas. Oma en presence d'excitations harmoniques : etude de cas sur des composantes de turbine hydroelectrique. *24th Seminar on Machinery Vibration*, October 2006.

[20] D. Valentin, A. Presas, M. Bossio, and M. Egusquiza Montagut. Feasibility to detect natural frequencies of hydraulic turbines under operation using strain gauges. *Sensors*, January 2018.

[21] A. Presas, D. Valentin, E. Egusquiza, and C. Valero. Detection and analysis of part load and full load instabilities in a real francis turbine prototype. *J. Phys.: Conf. Ser. 813 012038*, April 2017.

[22] D. Liu, X. Lui, and Y. Zhao. Experimental investigation of inter-blade vortices in a model francis turbine. *Chinese Journal of Mechanical Engineering vol. 30*, February 2016.

[23] R. Goyal and B.K. Gandhi. Review of hydrodynamics instabilities in francis turbine during off-design and transient operations. *Renewable Energy vol. 116*, page 697 to 709, October 2017.

[24] X. Liu, Y. Luo, and Z. Wang. A review on fatigue damage mechanism in hydro turbines. *Renewable and Sustainable Energy Reviews vol. 54*, February 2016.

[25] A. Gagnon, A. Tahan, P. Bocher, and D. Thibault. Influence of load spectrum assumptions on the expected reliability of hydroelectric turbines: A case study. *Structural Safety, vol. 50*, March 2014.

[26] X. Huang, J. Chamberland-Lauzon, C. Oram, A. Klopfer, and N. Ruchonnet. Fatigue analyses of the prototype francis runners based on site measurements and simulations. *IOP Conf. Ser.: Earth Environ. Sci. vol. 22 012014*, 2014.

[27] U. Seidel, C. Mende, B. Hubner, W. Weber, and D. Otto. Dynamic loads in francis runners and their impact on fatigue life. *IOP Conf. Ser.: Earth Environ. Sci. vol. 22 032054*, 2014.

[28] C. Trivedi, B. Gandhi, and M.J. Cervantes. Effect of transients on francis turbine runner life: a review. *Journal of Hydraulic Research vol. 51-2*, page 121 to 132, 2013.

[29] F. Leonard. Spectrogramme de phase et spectrogramme de frequence. *Traitement de signal vol. 17 nb 4*, page 269 to 286, 2000.

[30] F. Leonard. Phase spectrogram and frequency spectrogram as new diagnostic tools. *Mechanical Systems and Signal Processing vol. 21*, page 125 to 137, January 2007.

[31] P. Dorfler, M. Sick, and A. Coutu. Flow-induced pulsation and vibration in hydroelectric machinery. *Engineer's Guidebook for Planning, Design and Troubleshooting*, April 2012.

[32] G. Blommaert. Etude du comportement dynamique des turbines francis : controle actif de leur stabilite de fonctionnement. *These de l'Université Polytechnique Federale de Lausanne*, 2000.

[33] A. Favrel, C. Landry, A. Muller, and F. Avellan. Experimental identification and study of hydraulic resonance test rig with francis turbine operating at partial load. *IOP Conf. Ser.: Earth Environ. Sci. vol. 15 062064*, August 2012.

[34] A. Favrel, C. Landry, A. Muller, K. Yamamoto, and F. Avellan. Hydro-acoustic resonance behavior in presence of a precessing vortex rope: observation of a lock-in phenomenon at part load francis turbine operation. *IOP Conf. Ser.: Earth Environ. Sci. vol. 22 032035*, September 2014.

[35] C. Nicolet, N. Ruchonnet, S. Alligne, J. Koutnik, and F. Avellan. Hydroacoustic simulation of rotor-stator interaction in resonance conditions in francis pump-turbine. *IOP Conf. Ser.: Earth Environ. Sci. vol. 12 012005*, 2010.

[36] H. Tanaka. Vibration behavior and dynamic stress of runners of very high head reversible pump-turbines. *International Journal of Fluid Machinery and Systems vol.4*, page 289 to 306, June 2011.

[37] J. Blough, D. Brown, and H. Vold. The time variant discrete fourier transform as an order tracking method. *SAE Noise and Vibration Conf. and Exp.*, May 1997.

[38] P. Borghesani, P. Pennachi, S. Chatterton, and R. Ricci. The velocity synchronous discrete fourier transform for order tracking in the field of rotating machinery. *Mechanical Systems and Signal Processing vol. 44*, page 118 to 133, February 2014.

[39] D.B. Stephens and H. Vold. Order tracking signal processing for open rotor acoustics. *Journal of Sounds and Vibration vol. 333*, page 3818 to 3830, August 2014.

[40] E. Di Lorenzo. Operational modal analysis for rotating machines, challenges and solutions. *PhD - KL Arenberg Doct. School and Frederico II Naple Univ.*, April 2017.

[41] K.R. Fyfe and D.S. Munck. Analysis of computed order tracking. *Mechanical Systems an Signal Processing vol. 11*, page 187 to 205, March 1997.

[42] K. Janssens, Z. Kollar, B. Peeters, S. Pauwels, and H. Van der Auweraer. Order-based resonance identification using operational polymax. *ResearchGate Article*, January 2006.

[43] E. Di Lorenzo, S. Manzato, A. Dabizzi, B. Peeters, F. Marulo, and W. Desmet. Industrial applications of advanced modal identification on operational rotating machineries. *Proceeding of ISMA*, page 2833 to 2848, September 2016.

[44] E. Di Lorenzo, A. Palermo, S. Manzato, A. Dabizzi, B. Peeters, W. Desmet, and F. Marulo. Gear dynamics characterization by using order-based modal analysis. *Proceedings of the International Modal Analysis Conference (IMAC)*, page 387 to 404, 2016.

[45] H. Van der Auweraer, P. Mas, B. Peeters, K. Jannsens, and A. Vecchio. Modal and path contribution models from in-operation data: Review and new approaches. *Shock and Vibration vol. 15*, page 403 to 411, 2008.

[46] A.G. Poulimenos and S.D. Fassois. Parametric time-domain methods for non-stationary random vibration modelling and analysis : A critical survey and comparison. *Mechanical Systems and Signal Processing vol. 20*, page 764 to 816, January 2006.

[47] L. Ljung. System identification. *University of Linkoping, Sweden*, 1998.

[48] R Brinker and C.E. Ventura. Introduction to operational modal analysis. *Wiley Editions*, 2015.

[49] B. Peeters, H. Van der Auweraer, P. Guillaume, and J. Leuridan. The polymax frequency-domain method: a new standard for modal parameter estimation? *Shock and Vibration vol. 11*, page 395 to 409, August 2004.

[50] R. Brinker, L. Zhang, and P. Andersen. Modal identification from ambiant responses using frequency domain decomposition. *Proceedings of the International Modal Analysis Conference (IMAC)*, page 625 to 630, February 2000.

[51] R. Brinker, L. Zhang, and P. Anderser. Modal identification of output-only systems using frequency domain decomposition. *Smart Materials and Structures vol. 10*, page 441 to 445, January 2001.

[52] L. Zhang, T. Wang, and Y. Tamura. A frequency-spatial domain decomposition (fsdd) method for operational modal analysis. *Mechanical Systems and Signal Processing vol. 24*, page 1227 to 1239, July 2010.

[53] C.-X. Qu, T.-H. Yi, H.-N. Li, and B. Chen. Closely spaced modes identification through modified frequency domain decomposition. *Measurement vol. 128*, page 388 to 392, November 2018.

[54] M. Pastor, M. Binda, and T. Harcarik. Modal assurance criterion. *Procedia Engineering vol. 48*, page 543 to 548, 2012.

[55] R. Brinker, P. Andersen, and N.-J. Jacobsen. Automated frequency domain decomposition for operational modal analysis. *Proceedings of the International Modal Analysis Conference (IMAC)*, 2007.

[56] M. Danial, A. Hasan, Z.A.B. Ahmad, M. Salman Leong, and L.M. Hee. Enhanced frequency domain decomposition algorithm: a review of a recent development for unbiased damping ratio estimates. *Journal of Vibro-Engineering vol. 20*, page 1919 to 1936, August 2018.

[57] R. Castiglione, J. Antoni, and L. Garibaldi. Separation and identification of structural modes in largely underdetermined scenarios using frequency banding. *Journal of Sound and Vibration, vol. 414*, page 192 to 217, February 2018.

[58] S.-K. Au. Operational modal analysis, modeling, bayesian inference, uncertainty laws. *Springer*, 2017.

[59] J.A. Nelder and R. Mead. A simplex method for function minimization. *Computer Journal vol. 7*, page 308 to 313, 1965.